Journal of Power Sources 237 (2013) 64–73

Contents lists available at SciVerse ScienceDirect

Journal of Power Sources

journal homepage: www.elsevier.com/locate/jpowsour

Review

Gas transport in porous electrodes of solid oxide fuel cells: A review on diffusion and diffusivity measurement

Weidong He [a,b,*], Jing Zou [c], Bin Wang [d], Subramanian Vilayurganapathy [e], Ming Zhou [f], Xiao Lin [g], Kelvin H.L. Zhang [h], Junhao Lin [d], Ping Xu [i], James H. Dickerson [b,d,j]

[a] Interdisciplinary Program in Materials Science, Vanderbilt University, Nashville, TN 37235, USA
[b] Vanderbilt Institute of Nanoscale Science and Engineering, Vanderbilt University, Nashville, TN 37235, USA
[c] Department of Chemical Engineering, Pohang University of Science and Technology, San 31, Hyoja-dong, Nam-gu, Pohang, Gyungbuk 790-784, South Korea
[d] Department of Physics and Astronomy, Vanderbilt University, Nashville, TN 37235, USA
[e] Western Michigan University, 1903 West Michigan Ave., Kalamazoo, MI 49008, USA
[f] Department of Chemistry, The University of Hong Kong, Pokfulam Road, Hong Kong, PR China
[g] School of Physics, University of Chinese Academy of Sciences, Beijing 100049, PR China
[h] Department of Chemistry, Chemistry Research Laboratory, University of Oxford, Mansfield Road, Oxford OX1 3TA, United Kingdom
[i] Department of Chemistry, Harbin Institute of Technology, Harbin 150001, PR China
[j] Department of Chemistry, Vanderbilt University, Nashville, TN 37235, USA

HIGHLIGHTS

- Reviews models for gas transport in electrodes of solid oxide fuel cells (SOFCs).
- Discusses recently-developed devices for direct diffusivity measurement in SOFCs.
- Shows that diffusivity measurement facilitates the research on SOFC electrodes.

GRAPHICAL ABSTRACT

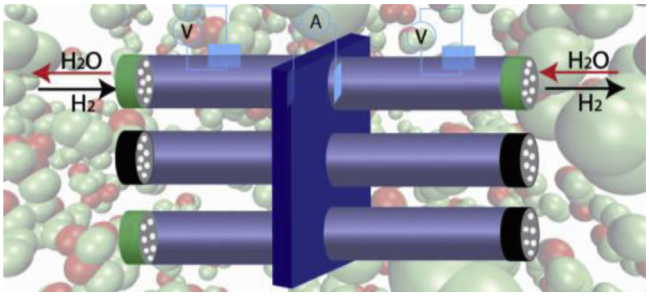

ARTICLE INFO

Article history:
Received 23 August 2012
Received in revised form
16 January 2013
Accepted 28 February 2013
Available online 28 March 2013

Keywords:
Solid oxide fuel cell
Porous electrodes
Gas diffusion
Diffusivity measurement
Concentration polarization

ABSTRACT

A reduction in Ohmic, activation and concentration-polarization losses is of paramount importance in improving the efficiency of solid oxide fuel cells, proton-exchange-membrane fuel cells, and molten-carbonate fuel cells. Efficient measurements of gas diffusivities at the operating conditions of fuel cells allow concentration polarization losses of these fuel cells to be reliably evaluated. To enhance the applicability of solid oxide fuel cells, tremendous work on the development of gas diffusion models and gas diffusivity measurement techniques have been done to pre-evaluate the concentration polarization losses of fuel cells. This review focuses on the recent advancement of gas diffusion models and diffusivity measurement techniques of solid oxide fuel cells. The review seeks to provide an insightful guidance for designing high-performance solid oxide fuel cell electrodes with efficient thickness, porosity, among other parameters.

1. Introduction

As the global population and economy continue to expand, a lot of attention is focused on improving the performance of existing

* Corresponding author. Interdisciplinary Program in Materials Science, Vanderbilt University, Nashville, TN 37235, USA. Tel.: +1 6153647338; fax: +1 6153437263.
E-mail address: weidong.he@vanderbilt.edu (W. He).

0378-7753/$ – see front matter © 2013 Elsevier B.V. All rights reserved.
http://dx.doi.org/10.1016/j.jpowsour.2013.02.089

energy systems as well as exploring new forms of sustainable energy sources [1–13]. One of the main proposed strategies toward sustainable energy sources is hydrogen-fuel based fuel cells, such as proton exchange membrane fuel cells (PEMFCs), molten carbonate fuel cells (MCFCs), and solid oxide fuel cells (SOFCs). Fuel cells directly convert stored chemical energy of fuels into electrical energy without combustion, and are capable of overcoming the combustion efficiency limitation as imposed by the Carnot cycle. Moreover, fuel cells reduce the emission of pollutants like nitrogen oxides (N_xO_y) and hence are environmentally friendly. Compared with other types of fuel cells, solid oxide fuel cells exhibit excellent fuel flexibility, and many chemicals including hydrogen, hydrocarbons, carbon monoxide and carbon, can be utilized as fuels [14–30].

There are mainly three types of energy losses associated with a fuel cell, i.e., activation loss (AL), concentration polarization (CP), and Ohmic loss (OL). Research has gained remarkable success in increasing the efficiency of SOFCs, the energy losses can be controlled well below 30%. The main drawback of SOFCs is their high operating temperatures, which are typically above 500 °C. At these temperatures, only a few materials can be employed as electrolytes and electrodes. This leads to an increase in cost, and hinders potential applications in portable and automobile power source. On the other hand, the concentration polarization of SOFCs typically increases as the operating temperature decreases [31,32]. Lowering the operation temperatures of SOFCs while maintaining a high efficiency has become the key focus in the SOFC field [33–40]. Toward this direction, new nanostructured electrodes composed of existing electrode materials, have been studied for potential applications in SOFCs [28,41–49]. In addition to materials development, efficient methods are required to pre-evaluate an electrode before it is assembled into a fuel cell. In particular, measuring the gas diffusivity in an electrode is considered to be an important aspect in facilitating such an evaluation since gas diffusivity correlates with both polarization loss and electrode parameters including porosity, thickness and tortuosity. Recently, gas diffusivity measurement techniques have undergone significant improvement, which has facilitated the efficient pre-evaluation of the polarization loss of SOFC electrodes in an out-of-cell fashion [50–53].

In this review, an overview on existing mechanisms and mathematical models of fuel gas transport through porous electrodes is presented, followed by a discussion on gas diffusivity. We then systematically investigate the efficiency of recently-developed electrochemical devices for direct diffusivity measurements and concentration polarization evaluation. We conclude by providing prospectives on possible future developments of gas transport models and further improvement of gas diffusivity measurements. The review and prospectives aim to enhance the performance of SOFCs by improving diffusivity measurement techniques and by pre-evaluating the parameters associated with micro/nano-porous electrodes.

2. Fuel gas diffusion models

In a fuel cell, oxygen molecules diffuse in the cathode, and are reduced to oxygen ions at the cathode active layer. These oxygen ions then transport through the electrolyte and react with the fuel gas at the anode/electrolyte interface to produce electricity. The driving force of a fuel cell is provided by the anode/cathode reaction. For a gas-based solid oxide fuel cell to operate, the activation energy of the anode/cathode reaction has to be overcome [54–57]. The pressure gradient of anode/cathode gas and the concentration gradient of oxygen ions across the anode/cathode and the electrolyte are determined by the transport rates of these gaseous and ionic species. While providing electricity, electrical resistance is also present in all operating components of the fuel cell [58–60]. Despite the high efficiency of existing SOFCs, there is still room for efficiency improvement. Moreover, an improvement of the cost effectiveness, even by a small amount, is crucial to the implementation of SOFCs in applications [1,61–64]. Fig. 1 shows a demonstration of concentration polarization loss, Ohmic loss, and activation loss associated with different components of a fuel cell. Ohmic loss due to electrical resistance is present across all fuel cell components whereas activation loss is induced by offsetting energy barrier for catalytic reactions at electrode/electrolyte interfaces. Concentration polarization is induced by the pressure gradient due to limited transport rates of gaseous reactant and/or product species through SOFC electrodes [31,50,51,61]. The chemical potential of a mass system is the function of the concentration/density of the mass species, and can be expressed by Eq. (1),

$$\mu_i = \mu_o + RT\ln n_i \quad (1)$$

where μ_i is the chemical potential of species i at a given state, R is gas constant, T is temperature, and n_i is the concentration of species i. CP is induced by the chemical potential gradient due to diffusion-limited gas transport through electrodes.

A thorough understanding of the gas transport mechanism along with an accurate calculation or measurement of CP at operating conditions is important for reducing polarization losses in SOFCs. The one-dimensional diffusion of gas fuel molecules in porous media involves molecular interactions between gas molecules as well as collisions between gas molecules and the porous media [65–67]. As gas fuel molecules, such as H_2, and CH_4, transport through the porous anode of an SOFC, one of three mechanisms can occur, depending on the characteristic of the diffusing gas species and the intrinsic microstructure of the anode [67]. The three mechanisms are molecular diffusion, viscous diffusion, and Knudsen diffusion. To distinguish the three mechanisms, Knudsen number (K_n), the ratio of the gas mean free path to the size of pores of an electrode, is typically used [66–68]. If K_n is much greater than 10, collisions between gas molecules and a porous electrode are more dominant than the collisions between gas molecules resulting in negligible molecular diffusion as well as viscous diffusion. If K_n is much smaller than 0.1, collisions and interactions between gas molecules become dominant and Knudsen diffusion becomes negligible compared with molecular diffusion and viscous diffusion. When the K_n of a system ranges between 0.1 and 10, all the

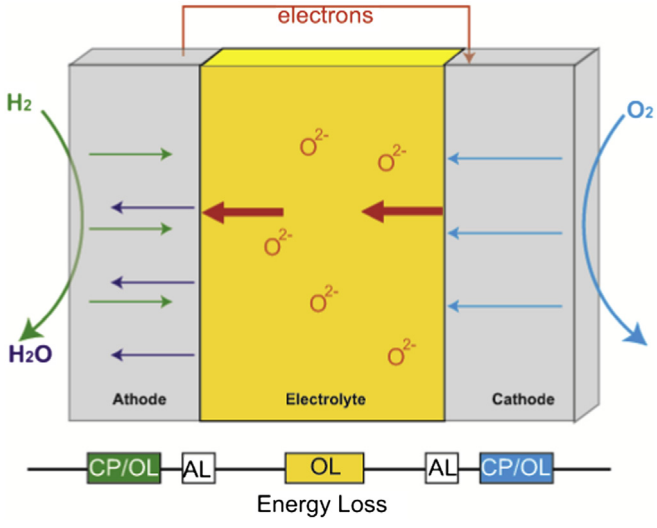

Fig. 1. Polarization losses and mass transfer associated with SOFC components.

three mechanisms govern gas transport. Different mathematical models have been developed to study the parameters associated with the three different mechanisms, including diffusion coefficient, gas flux and gas concentration [69,70]. In SOFC systems, the electrode pores vary from a few nanometers to several micrometers in size and the mean free path of fuel gas molecules is a few hundred nanometers. Therefore, K_n is in the range of 0.1–5, and all the three gas transport mechanisms must be considered and the different models must be comprehended to understand the gas transport of an SOFC system. Different theoretical models have been proposed to describe the gas transport of SOFC systems. Owing to inherent simplicity, Fick's law (FL) has been the most widely used diffusion-based model. FL is depicted in Eq. (2),

$$J_i = -\frac{D_i}{RT}\frac{c_i \partial(\mu_i)}{\partial x} \quad i = 1, 2, \ldots n \tag{2}$$

where J_i is the flux of gas species i, D_i is the diffusivity, R is gas constant, T is temperature, x is one-dimensional diffusion path, c_i is molar fraction of gas species i, and μ_i is chemical potential [71]. Fick's law only considers molecular diffusion, and assumes that the gas flux is proportional to gas pressure gradient. This drawback is addressed in the extended Fick's law which combines molecular diffusion modeled by Fick's law and viscous diffusion modeled by Darcy's law. The extended Fick's law also known as advective-diffusive model (ADM), is expressed in Eq. (3),

$$J_i = -\frac{k}{\mu_g}\rho_g \omega_i \nabla P_g - D_{12}\rho_g \nabla \omega_i \tag{3}$$

where k is effective permeability, μ_g is gas viscosity, ρ_g is gas density, D_{12} is binary gas diffusivity, ω_i is mass fraction of gas species i, and P_g is gas pressure [72]. Both FL and ADM only take into account unidirectional interactions in simple dilute binary gas systems; neither of them is valid for ternary or concentrated gas systems where molecular interactions cannot be neglected. To model such complicated systems, the Maxwell–Stefan model (MSM) was developed, which is shown in Eqs. (4) and (5),

$$\frac{dy_i}{dz} = \sum_{j=1}^{n} \frac{y_i N_j - y_j N_i}{C D_{i,j}} \quad i = 1, 2, \ldots, n \tag{4}$$

$$\frac{dy_i}{dz} = \sum_{j=1}^{n} \frac{y_i N_j - y_j N_i}{C D_{i,j}^{\text{eff}}} \quad i = 1, 2, \ldots, n \tag{5}$$

where y_i is the mole fraction of gas species i, C is total concentration, $D_{i,j}$ is Maxwell–Stefan diffusivity, N_i is molar flux of gas species i, and $D_{i,j}^{\text{eff}}$ is effective gas diffusivity [73]. MSM can successfully model gas transport in uniform media or in electrostatic fields. However, MSM fails to model gas systems where gas species frequently collide with the porous media. To model such gas systems accurately, a dusty gas model (DGM) was developed, which is shown in Eqs. (6) and (7),

$$\sum_{j=1, j\neq 1}^{n} \frac{x_i N_j^D - x_j N_i^D}{D_{ij}} - \frac{N_i^D}{D_{iK}} = \frac{P_g \nabla x_i}{RT} + \frac{x_i \nabla P_g}{RT} \tag{6}$$

$$\sum_{j=1, j\neq 1}^{n} \frac{x_i N_j^T - x_j N_i^T}{D_{ij}} - \frac{N_i^T}{D_{iK}} = \frac{P_g \nabla x_i}{RT} + \left(1 + \frac{k_0 P_g}{D_{iK}\mu_g}\right)\frac{x \nabla P_g}{RT} \tag{7}$$

where x is gas mole fraction, N_j^D is diffusive molar flux of gas species j, N_j^T is total diffusive and advective molar flux, P_g is total gas pressure, R is gas constant, T is temperature, D_{ij} is binary diffusivity in free space, and D_{iK} is Knudsen diffusivity of gas species i [74]. The DGM model considers all possible interactions and collisions, and exhibits high accuracy while modeling gas fuel transport through porous fuel cell electrodes. However, DGM has not been as widely used as FL due to its complexity in modeling multicomponent gas fuel systems. The accuracy of DGM coupled with the simplicity of FL, yielded the recently developed DGM–FL, which is a more practical gas diffusion model. The model is expressed in Eq. (8),

$$J_l = J_l^{\text{diffusion}} + J_l^{\text{convection}} = -\overline{D_2}\nabla \overline{c_2} - \overline{c_2}\frac{\overline{k_2}}{\mu}\nabla p \tag{8}$$

where $\overline{D_2}$, $\overline{c_2}$, and $\overline{k_2}$ are simplified diffusivity, molar concentration, and permeability of gas species, μ is chemical potential, and p is gas pressure [75]. DGM–FL was obtained by deriving DGM in the FL form. This approach results in a simple, efficient and reliable model of a typical gas transport system. In order to account for both Knudsen and viscous effects simultaneously, a binary friction model (BFM) was derived, as shown in Eq. (9),

$$\frac{dp}{dx} = -RTN\left(D_K^{\text{eff}} + \frac{B_v p}{\eta}\right)^{-1} \tag{9}$$

where p is gas pressure, $N$is net gas transport, D_K^{eff} is Knudsen diffusivity, B_v is viscous permeability, and η is the viscosity of the gas species [76,77]. Compared to Darcy's law which only takes viscous effects into account, BFM shows improved accuracy when it is employed to model gas transport phenomena in fuel cells [78].

In the discussed models, the term "effective gas diffusivity" was mentioned. We need to look into multicomponent diffusion in more details to comprehend the term. Effective binary gas diffusivity was introduced to simplify computations on the diffusion parameters of a multicomponent gas system since the values of diffusion fluxes at various locations and time points are often required to understand the gas transport in a fuel cell system [50,58,79]. In the effective binary diffusion, a multicomponent gas system is approximated as a binary mixture of gas species i and a composite gas species corresponding to all the other gas species in the system. By introducing effective binary gas diffusivity, any multicomponent gas system can be conveniently treated as a binary gas system. As molecular diffusion, viscous diffusion, and Knudsen diffusion are all considered, the flux of an isothermal binary gas system, such as O_2/N_2 and H_2/H_2O, can be modeled by Eqs. (10) and (11),

$$J_1 = -D_1 \nabla n_1 + X_1 \delta_1 J - X_1 \gamma_1 \left(\frac{nB_o}{\mu}\right)\nabla p \tag{10}$$

$$J_2 = -D_2 \nabla n_2 + X_2 \delta_2 J - X_2 \gamma_2 \left(\frac{nB_o}{\mu}\right)\nabla p \tag{11}$$

where

$$\delta_1 = 1 - \gamma_1 = \frac{D_{1K}^{\text{eff}}}{D_{1K}^{\text{eff}} + D_{12}^{\text{eff}}} \text{ and } \delta_2 = 1 - \gamma_1 = \frac{D_{2K}^{\text{eff}}}{D_{2K}^{\text{eff}} + D_{12}^{\text{eff}}} \tag{12}$$

$$\frac{1}{D_1} = \frac{1}{D_{1K}^{\text{eff}}} + \frac{1}{D_{12}^{\text{eff}}} \text{ and } \frac{1}{D_2} = \frac{1}{D_{2K}^{\text{eff}}} + \frac{1}{D_{12}^{\text{eff}}} \tag{13}$$

where J_1 and J_2 are the fluxes of gas species 1 and 2, J is the total flux, n_1 and n_2 are the concentrations of gas species 1 and 2, n is the total gas concentration, X_1 and X_2 are the molar fractions of gas species 1 and 2, μ is viscosity, B_o is permeability, P is total pressure,

D_{1K}^{eff} and D_{2K}^{eff} are the effective Knudsen diffusivities of gas species 1 and 2, and D_{12}^{eff} is the effective binary diffusivity [50].

3. Fuel gas diffusivity measurements

The polarization losses in SOFCs, CP, OL, and AL were typically obtained via fittings on multiple voltage–current (V–I) data measured in operating conditions according to Eq. (14),

$$E(i) = E_o - iR_i - \frac{2RT}{F}\ln\left\{\frac{1}{2}\left[\left(\frac{i}{i_o}\right) + \sqrt{\left(\frac{i}{i_o}\right)^2 + 4}\right]\right\} + \frac{RT}{2F}\ln\left(1 - \frac{i}{i_{\text{as}}}\right) - \frac{RT}{2F}\ln\left(1 + \frac{p_{\text{H}_2}^o i}{p_{\text{H}_2\text{O}}^o i_{\text{as}}}\right) + \frac{RT}{4F}\ln\left(1 - \frac{i}{i_{\text{cs}}}\right) \quad (14)$$

where E_o is open circuit potential, R_i is Ohmic resistance, F is Faraday constant, p is gas pressure, i_o is exchange current density, i_{as} is anode limiting current density, i_{cs} and is cathode limiting current density [39]. While this method is mathematically feasible, the accuracy of fitting five parameters based on a limited number of measurements is debatable. The correlation between concentration polarization and limiting current density is shown in Eqs. (15) and (16) [52,53].

$$\eta_{\text{anode}} = -\frac{RT}{2F}\ln\left(1 - \frac{i}{i_{\text{as}}}\right) + \frac{RT}{2F}\ln\left(1 + \frac{p_{\text{H}_2}^o i}{p_{\text{H}_2\text{O}}^o i_{\text{as}}}\right) \quad (15)$$

$$\eta_{\text{cathode}} = -\frac{RT}{4F}\ln\left(1 - \frac{i}{i_{\text{cs}}}\right) \quad (16)$$

Limiting current density is a function of the diffusion coefficient associated with anode/cathode gas transport, i.e., diffusivity, as shown in Eqs. (17) and (18),

$$i_{\text{as}} \approx \frac{4\text{F}p_{\text{H}_2}^o \phi_a D_{\text{H}_2-\text{H}_2\text{O}}^{\text{eff}}}{RTl_a\tau_a} \quad (17)$$

$$i_{\text{cs}} \approx \frac{8\text{F}p_{\text{O}_2}^o \phi_c D_{\text{O}_2-\text{N}_2}^{\text{eff}}}{RTl_c\tau_c}\left(\frac{P_t}{P_t - P_{\text{O}_2}^o}\right) \quad (18)$$

where F is Faraday constant, $\phi_a(\phi_c)$ is anode (cathode) porosity, $D_{\text{H}_2-\text{H}_2\text{O}}^{\text{eff}}\cdot(D_{\text{O}_2-\text{N}_2}^{\text{eff}})$ is effective binary diffusivity of H_2/H_2O (O_2/N_2) gas, $l_a(l_c)$ is anode (cathode) thickness, and $\tau_a(\tau_c)$ is anode (cathode) tortuosity [61]. With known diffusivity, the anode/cathode concentration polarization can be directly calculated. Further, the electrodes are rendered useless if the anode/cathode diffusivity obtained from V–I measurements conducted on intact fuel cells is below an expected value. Therefore, the direct measurement of gas diffusivity in an out-of-cell fashion is highly cost-effective [51].

Recently, different techniques have been developed to measure gas diffusivity in fuel cells. Although each measurement device was designed for a specific type of fuel cell, these devices could be employed for the gas diffusivity measurements in other types of fuel cells due to their similarity in fuel types and architectural designs. Therefore an overview of gas diffusivity measurement techniques in other fuel cells, such as PEMFCs, is beneficial for the development of gas diffusivity measurements and energy loss evaluation in SOFCs. For PEMFCs, three types of measurement devices have been investigated recently. Fig. 2 shows a self-heated oxygen sensor device for the gas diffusivity measurement in PEMFCs [80].

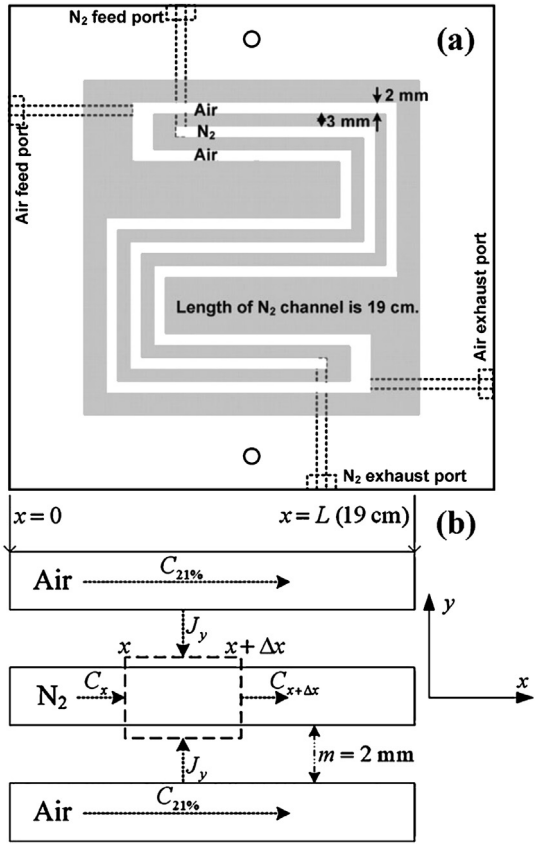

Fig. 2. (a) Plan view of a self-heated oxygen sensor device (b) schematic of oxygen mass balance through N_2 channel [80].

N_2 and air channels were used in the device to create oxygen pressure gradient and oxygen diffusion through the electrode between the two channels. With given electrode thickness (δ), diffusive length, width (m) of the sealing gasket used in the device, gas flow rate, and oxygen pressure at the exhaust port, the gas diffusivity can be calculated through Eq. (19),

$$D_{\text{O}_2}^{\text{eff}} = \frac{mQC_{x=L}}{2\delta LC_{\text{air}}} \quad (19)$$

where $C_{x=L}$is molar oxygen concentration at the exhaust of N_2 channel, and C_{air} is molar oxygen concentration at the exhaust of N_2 channel in the air channel. Another type of gas diffusivity measurement device based on a modified Loschmidt cell is shown in Fig. 3 [81].

For a given value of oxygen pressure in the device, measured with the oxygen probe, the effective diffusion coefficient of a porous layer is obtained via Eq. (20),

$$D_i^{\text{eff},1} = \frac{L_2 - L_0}{H/D_i^{\text{eq}} - (H - L_2 - L_0)/D_i^{\text{bulk}}} \quad (20)$$

where D_i^{eq} is the equivalent diffusivity of species i, obtained via Eq. (21) [82].

$$C_i = \frac{C_i^b}{2}\text{erfc}\left(\frac{H}{2\sqrt{\Delta t D_i^{\text{eq}}}}\right) \quad (21)$$

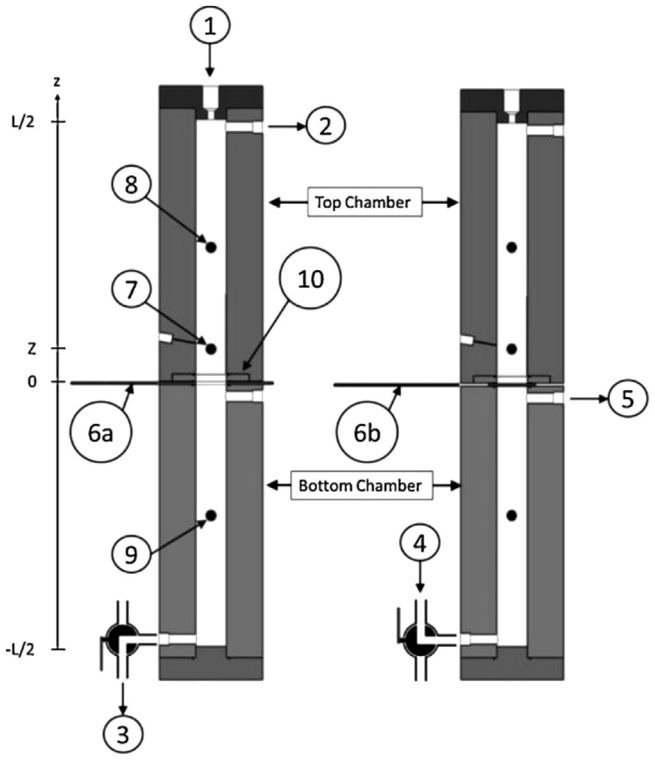

Fig. 3. Schematic of a modified Loschmidt cell for the measurement of effective diffusion coefficient. 1: Gas inlet 1; 4: gas inlet 4; 2, 3 and 5: outlets; 6: sliding gate valve; 6 (a): open position of the valve; 6 (b): closed position of the valve; 7: oxygen probe; 8 and 9: thermocouples; 10: sample holder [81].

In Eq. (16), D_i^{bulk} is the bulk diffusivity of species i, and can be calculated through Eq. (22) [83].

$$\ln D_i^{\text{bulk}} = 1.724 \ln T + \ln\left(1.13 \times 10^{-5}\right) - \ln p \tag{22}$$

Until now, only room temperature diffusivity has been measured using this device. However, owing to the robustness of its components, high temperature measurements are also possible with this device. Another device based on a modified diffusion bridge setup was recently employed to measure the Knudsen diffusivity and absolute permeability in PEMFC electrodes [78,83,84]. The schematic of the device is shown in Fig. 4. A porous electrode is sandwiched between two gas channels. A gas pressure transducer was employed to trace the pressure gradient of gas diffusion through the porous electrode. A BFM model was employed to calculate the gas diffusivity, as well as the correlation between absolute permeability and gas diffusivity [78]. Here, we propose that, by replacing the components with high-temperature ceramics, the different devices for gas diffusivity measurement in PEMFCs should be employed for gas diffusivity measurements in SOFCs. A review on recently-developed electrochemical devices for gas diffusivity measurements in SOFCs follows.

To facilitate the anode gas diffusivity measurement in SOFCs, an oxygen-sensor and oxygen-pump based electrochemical device, as shown in Fig. 5, was developed [71]. To make the device, a YSZ tube was employed, with a YSZ disc attached to one end and an anode/cathode sample attached to the other. An oxygen pump was employed to provide current across the YSZ disc. A voltage meter was used as an oxygen sensor to measure the oxygen pressure gradient across the YSZ tube. YSZ disc–YSZ tube and electrode–YSZ tube connections were accomplished by glass paste, and connection between wiring and YSZ was accomplished by Ni–YSZ paste and glue. The device was employed to measure the binary effective H_2/H_2O gas diffusivity in SOFCs at operating conditions. During the measurement, H_2O/H_2 was introduced into an air-tight tube furnace where the measurement setup was placed. Upon supply of a current via the oxygen pump, H_2/H_2O flux was induced through the anode sample at the other end of the YSZ tube. The correlation between the current supply and the induced flux is expressed by Eq. (23).

$$J_{H_2} = -J_{H_2O} = \frac{i}{4F} \tag{23}$$

Flux is a function of diffusivity and H_2 pressure gradient across the anode sample, as shown in Eq. (24),

$$J_{H_2} = \frac{i}{4F} = -D^{\text{eff}}_{H_2-H_2O} \nabla n_{H_2} = -\frac{D^{\text{eff}}_{H_2-H_2O}}{RT} \frac{dp_{H_2}}{dx} \tag{24}$$

where $D^{\text{eff}}_{H_2-H_2O}$ is the effective binary diffusivity of H_2 and H_2O, ∇n_{H_2} is concentration difference within dx, and dp_{H_2} is pressure gradient of H_2 within dx. Integration over H_2 pressure from one side of the anode sample to the other side of the anode sample leads to Eq. (25),

$$p^{(i)}_{H_2} = p^{o}_{H_2} = -\frac{RTl_a}{4FD^{\text{eff}}_{H_2-H_2O}} i \tag{25}$$

where $p^{(i)}_{H_2}$ is H_2 pressure in the YSZ tube, $p^{o}_{H_2}$ is H_2 pressure out of YSZ tube, l_a and is anode thickness.

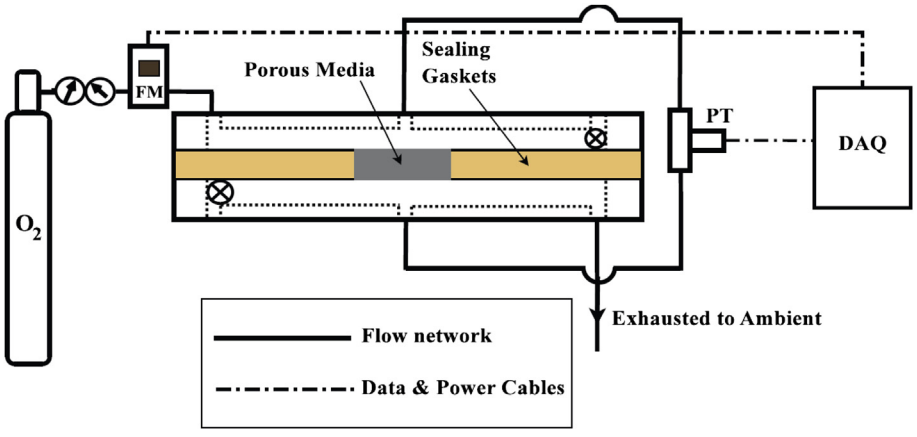

Fig. 4. Schematic of permeability measurement experimental setup, FM: mass flow controller; PT: differential pressure transducer; DAQ: data acquisition card [78].

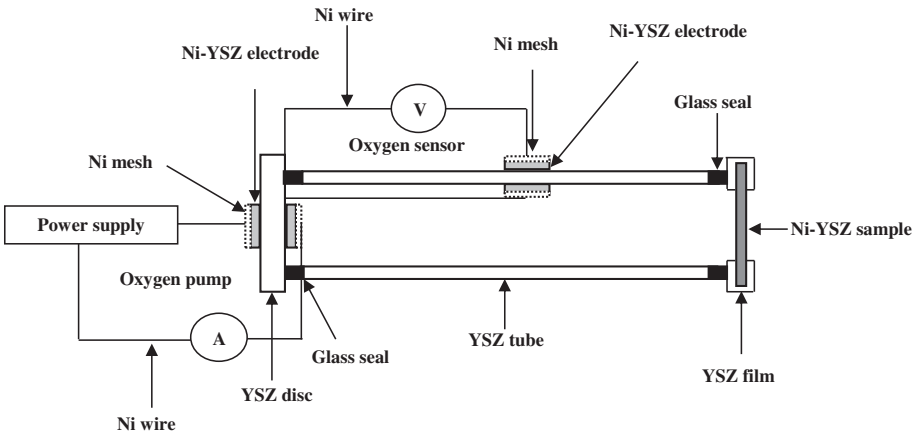

Fig. 5. A single-sensor electrochemical device for anode gas diffusivity measurement in SOFCs [51].

Eq. (25) shows that the H_2 pressure in the YSZ tube is a function of i. At a certain temperature, the reaction equilibrium constant for H_2O, H_2 and O_2 is fixed. With the pressure difference across the tube measured via the voltage meter, the effective binary H_2/H_2O diffusivity can be expressed by Eq. (25). With the measured diffusivity, anode concentration polarization loss as well as anode limiting current can be calculated based on Eqs. (15) and (17). The setup works highly efficiently; less than 5 min was sufficient for the sensor to read a stable voltage value. Fig. 6 shows a voltage curve measured with the oxygen sensor. Based on the measured equilibrium voltage value, the diffusivity, and concentration polarization were evaluated, as shown in Fig. 6b and c.

As shown in Fig. 6b, the measured diffusivity for 0.8 mm Ni/YSZ anode sample is proportional to $T^{3/2}$, which is consistent with Eq. (26),

$$D_{A-B} = \frac{0.00189T^{3/2}\left(\frac{1}{M_A}+\frac{1}{M_B}\right)^{1/2}}{p\Omega\sigma_{A-B}^2} \quad (26)$$

where M_A and M_B are the molecular weights of gaseous species A and B, Ω is collision integral, σ_{A-B} is average collision diameter, and p is total pressure of the system. As indicated by Eqs. (15) and (16), concentration polarization is a function of operating current density. According to Fig. 6c, for the specific anode sample in the report, a lower current appears to be more advantageous at 700 °C compared to 800 °C. Such an evaluation based on reliable diffusivity measurements is of practical importance in designing efficient operating temperatures for an anode prior to its assembly into an SOFC system.

Similar to the anode diffusivity measurement, a cathode diffusivity measurement has been conducted by Zhao et al., using an electrochemical cell [50]. Using the device, effective binary O_2–N_2 diffusivity was measured with O_2–N_2 flow at operating conditions. In the report, the correlation between concentration and other important parameters, such as cathode thickness, and porosity, were studied. For a specific porosity, CP increased with increasing cathode thickness, whereas at a fixed temperature and cathode thickness, CP decreases with increasing cathode porosity. Thus, the authors proposed using thin porous cathodes to improve O_2 diffusivity and in turn enhance the efficiency of SOFCs. The effective binary O_2–N_2 diffusivity was found to follow the law $D = aT^{3/2}$, where a is a constant that increases with decreasing cathode porosity. Gas diffusivity of high-porosity cathodes in SOFCs is less sensitive to the variation of operating temperature compared to low-porosity cathodes. Therefore, using highly-porous cathodes allows the operating temperature to be varied to meet practical requirements without increasing the concentration polarization during the operation of an SOFC [50].

Direct measurement of gas diffusivity in SOFCs via the single-sensor electrochemical cell greatly facilitates the efficient evaluation of an electrode before intact fuel cells are fabricated. However, the single-sensor electrochemical device is not highly efficient for diffusivity measurements. For example, only one sample can be tested at one time, and additional heating/cooling and gas switches are needed to measure additional electrodes. As noticed from Fig. 5, only one electrode sample is attached to the YSZ disc, leaving the other side of the YSZ disc un-utilized. The authors proposed that two YSZ tubes should be attached to both sides of the YSZ disc for simultaneous testing of two electrodes. [52]. Fig. 7 shows a schematic of the proposed device. The device doubled the efficiency of diffusivity measurements in SOFCs, and allowed one to evaluate electrode thickness more efficiently compared to the single-sensor electrochemical device.

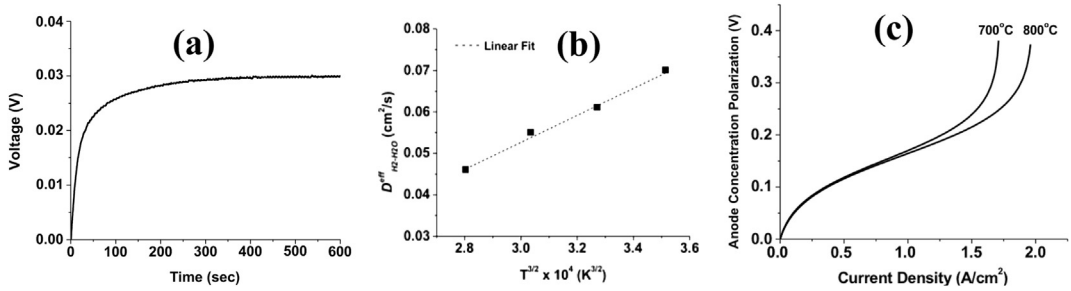

Fig. 6. (a) A voltage curve measured with the single-sensor electrochemical cell, (b) temperature dependence of anode gas diffusivity, and (c) correlation between anode concentration polarization and current density [51].

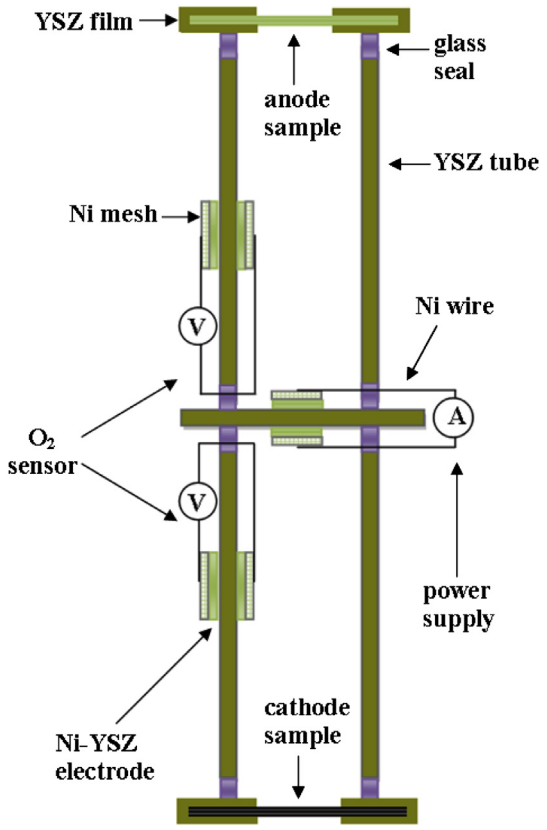

Fig. 7. A double-sensor electrochemical device for anode/cathode gas diffusivity measurement in SOFCs [52].

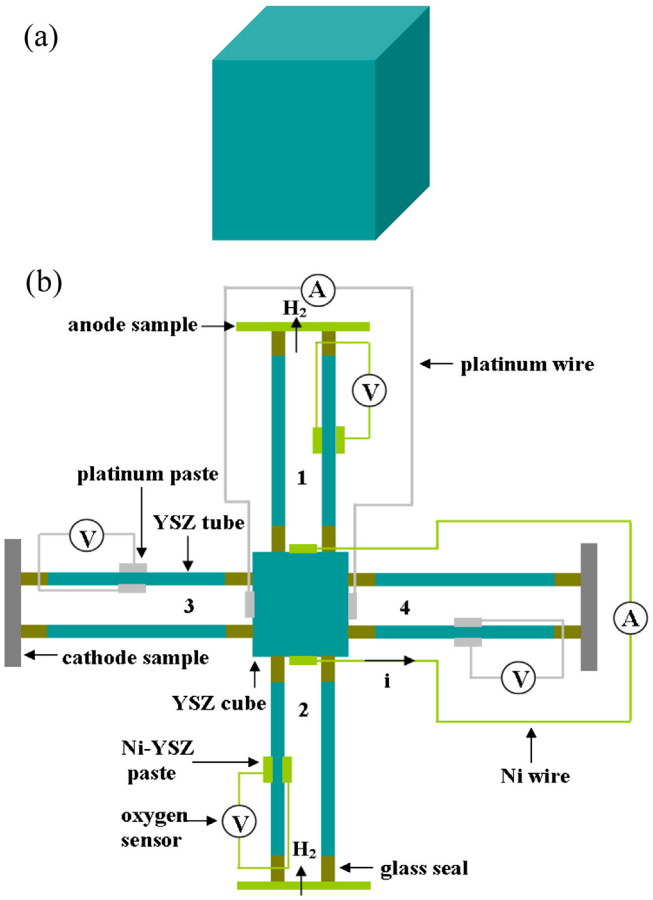

Fig. 9. A multi-sensor electrochemical device for anode/cathode gas diffusivity measurement in SOFCs: (a) a cube made of electrolyte material and (b) a plan view of the device [53].

The authors then studied the correlation between anode/cathode CP and electrode thickness. The plotted CP-thickness curves, displayed in Fig. 8 for 650 °C, 700 °C, 750 °C, and 800 °C, show crossing features for both cathodes and anodes. The findings were surprising because larger T typically resulted in smaller CP for SOFCs. For example, with fixed anode thickness of 0.5 mm, and applied current density of 0.05 A cm^{-2}, the anode CP at 750 °C was the largest, followed by the CPs at 800 °C, 700 °C, and 650 °C, respectively. For an anode thickness above 10 mm, anode CP increased with increasing operating temperature. Similar phenomenon was observed in cathode CP-versus-cathode-thickness plots. As seen in Fig. 8, anode CP appears to increase very rapidly with increasing anode thickness while cathode CP increases very gradually with increasing cathode thickness. Such findings are based on efficient diffusivity measurements with the double-sensor electrochemical device, and the findings provide an efficient platform for one to pre-evaluate anode/cathode thickness before the electrode is fabricated and assembled.

Compared to zero-dimensional single-sensor electrochemical cells and one-dimensional double-sensor electrochemical cells, two-dimensional and three-dimensional electrochemical cells should show higher efficiency for electrode diffusivity measurements in SOFCs. Further, increasing diffusivity measurement efficiency allows one to more extensively investigate CP and limiting current density with respect to other important parameters associated with fuel cells. A multi-sensor electrochemical device was designed by using a three-dimensional electrolyte cube, as shown in Fig. 9 [53]. For YSZ-based SOFCs, six YSZ tubes can be attached to the six sides of the cube, thereby enabling simultaneous testing of six electrodes.

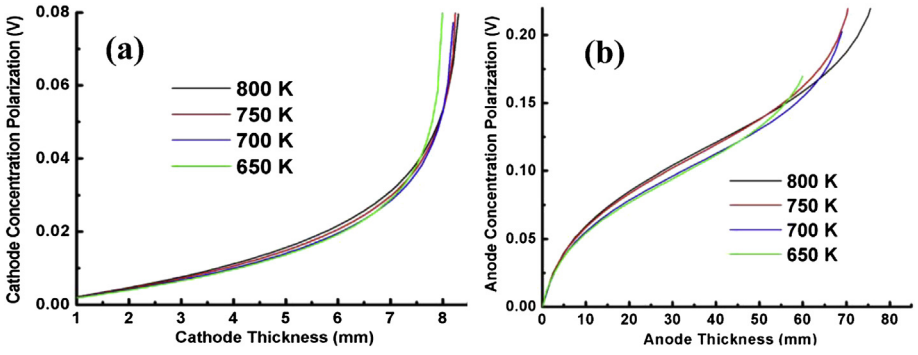

Fig. 8. (a) Correlation between CP and cathode thickness, and (b) correlation between CP and anode thickness [52].

With the efficiency of diffusivity measurement improved further with the above design, overall concentration polarization was evaluated with respect to electrode thickness, and crossing features were observed from overall CP-versus-thickness plots at 650 °C, 700 °C, 750 °C, and 800 °C for both anode and cathode samples. The crossing features imply that CP-versus-electrode thickness is temperature dependent, and that one must consider specific electrode thickness before choosing an operating temperature for an SOFC. Crossing features were also found in the overall CP-versus-current-density plots. This indicates that the CP-versus-temperature dependence is current–density dependent, and that the selection of efficient operating temperatures for fuel cells should be based on the current densities that are employed.

As discussed in the report, wiring connection can be challenging for such a three-dimensional device during actual measurements, and utmost care is necessary to avoid short-circuiting during measurements. As a solution to this potential problem, a recent report proposed the use of a two-dimensional YSZ plate instead of the three-dimensional YSZ cube [61]. With two-dimensional wiring connection, the device reduces the risk of short circuit during measurement to a large extent. As shown in Eq. (26), diffusivity is a function of electrode porosity. For a fixed tortuosity, operating temperature and thickness, diffusivity is linearly dependent on electrode porosity. Thus, direct measurement of gas diffusivity in an SOFC electrode largely facilitates the efficient evaluation of the correlation between concentration polarization and electrode porosity. The authors investigated the correlation between CP and porosity for fuel cells with nanostructured electrodes [61]. As noticed in Fig. 10, CP decreases with increasing the anode porosity for 10 nm, 100 nm, 500 nm, and 1000 nm thick anode samples at 650 °C, 700 °C, 750 °C, and 800 °C. The monotonous decrease of CP with an increase in electrode porosity suggests that high porosity is favored for improving the energy conversion efficiency of SOFCs.

Further, the authors defined critical porosity as the value where CP reaches a plateau, and remains unchanged with further increase in porosity. With a fixed applied current density of 0.05 A cm^{-2}, and an operating temperature of 700 °C, the critical porosity value for 10 nm thick electrodes is 0.15, followed by 0.4, and 0.7 for 100 nm, and 500 nm anodes, respectively. For 1000 nm anodes, no plateau is reached in the CP-versus-porosity plots. The results are consistent for all the four operating temperatures. Therefore, the use of thin nanostructured electrodes is highly recommended since only relatively low porosity is needed to achieve high SOFC efficiencies with such electrodes. In order to employ ultra-thin electrodes, the authors proposed using a thin coating as anode active layer and a mechanically strong material as anode support in real-life fuel cell applications [61].

As shown in Eqs. (17) and (18), the limiting current density of a fuel cell electrode decreases with increasing tortuosity of the electrode. Further, gas diffusivity is a function of tortuosity, as shown in Eqs. (27) and (28).

$$D^{\text{eff}}_{H_2-H_2O} = \frac{\phi_a}{\tau_a} D_{H_2-H_2O} \tag{27}$$

$$D^{\text{eff}}_{O_2-N_2} = \frac{\phi_c}{\tau_c} D_{O_2-N_2} \tag{28}$$

For most porous fuel cell electrodes, the value of tortuosity ranges from 2 to 25 and fuel cell performance can be improved by tuning the tortuosity values of the fuel cell electrodes within or beyond the range [51]. In the authors' recent work, the correlation between effective binary gas diffusivity and electrode tortuosity is studied [85]. Fig. 11 shows the electrode diffusivity versus

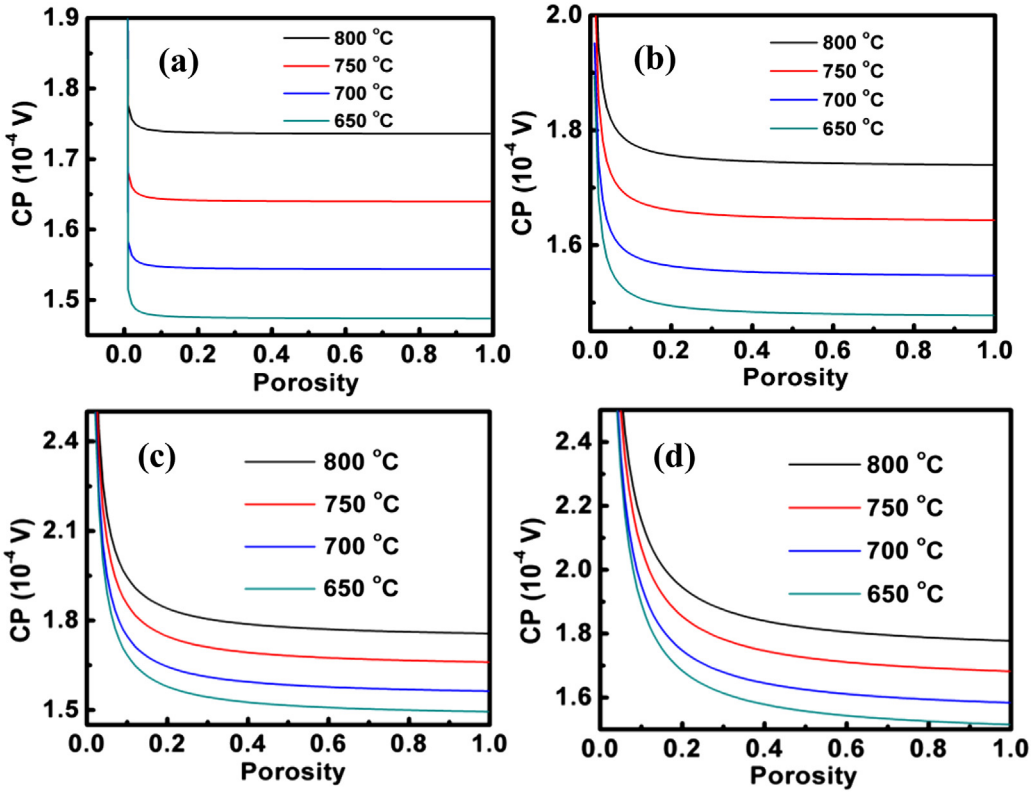

Fig. 10. Correlation between CP and anode porosity for (a) anode thickness: 10 nm, (b) anode thickness: 100 nm, (c) anode thickness: 500 nm, and (d) anode thickness: 1000 nm [61].

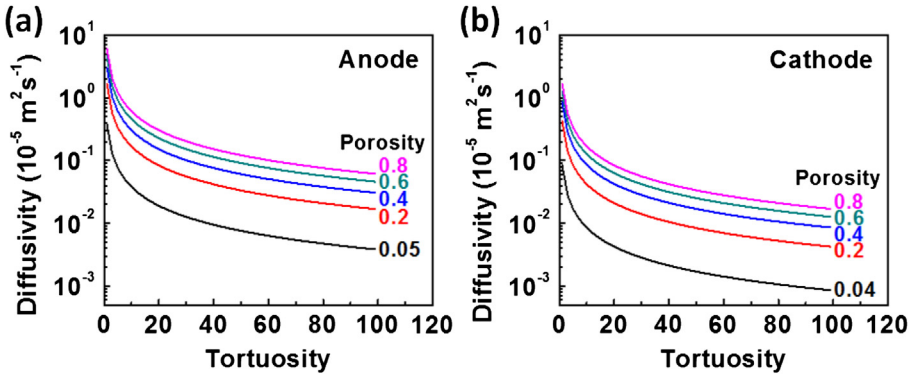

Fig. 11. The plots of anode (a)/cathode (b) effective binary diffusivity versus tortuosity with different electrode porosities, and a fixed electrode thickness of 1 mm [85].

tortuosity plots for different electrode porosities. For both anodes and cathodes, diffusivity increases with decreasing tortuosity. Below a certain tortuosity, diffusivity increases rapidly and then reaches an infinite value. The critical tortuosity increases with the increase of electrode porosity; thus, to increase gas diffusivity it is more efficient to decrease the tortuosity of an electrode with larger porosity than decreasing the tortuosity of an electrode with smaller porosity. Comparing with the diffusivity versus tortuosity plots for anodes, diffusivity versus tortuosity plots for cathodes appear to be more porosity-dependent, which indicates that increasing cathode porosity is more efficient to increase the gas diffusivity and to reduce the concentration polarization of a fuel cell system than increasing anode porosity.

4. Prospectives

For further advances in gas diffusivity measurement, the authors propose that several topics should be investigated. First, electrode and fuel gas systems with critical Knudsen numbers should be developed. At such critical Knudsen numbers, either collisions between fuel gas molecules or collisions between fuel gas molecules and porous electrodes become negligible [75]. The development of such systems will help to efficiently evaluate the suitability of the different gas transport models for a specific fuel gas/porous electrode system. Second, electrochemical devices should be designed to allow for the measurement of gas diffusivity in ultra-thin electrodes. The investigation will improve our understanding of gas diffusion on atomic/nanoscale levels. Another research direction is to measure gas diffusivity in three electrode directions using existing/improved gas diffusivity measurement devices. The study will largely improve our understanding on the correlation between 3D diffusivity and electrode parameters including porosity, tortuosity, Young modulus and microscopic roughness [86,87]. In the end, the review as presented here inspires the fuel cell community to develop cost-effective devices for highly-efficient ionic/electronic conductivity measurement. The effort will improve our general understanding of mass transport in fuel cells and help develop cost-effective fuel cells with highly-efficient electrodes, low-operating-temperature electrolytes, as well as low polarization loss [88,89].

5. Conclusion

In this review, the mechanisms and mathematical models of mass transport in porous SOFC electrodes have been discussed. Various diffusion models and mechanisms, as well as gas diffusivity measurement techniques have allowed polarization losses and limiting current densities of SOFCs to be reliably evaluated. Improved control over electrode microstructure will facilitate a more efficient modeling on gas diffusion in SOFCs. We are hopeful that direct diffusivity measurement techniques will continue to advance in the years to come. Such promising research trajectories will help to reduce the energy crisis faced by our society.

References

[1] J. Santamaria, J. Garcia-Barriocanal, A. Rivera-Calzada, M. Varela, Z. Sefrioui, E. Iborra, C. Leon, S.J. Pennycook, Science 321 (2008) 676–680.
[2] G.Q. Lu, Y. Jia, L.N. Cheng, N. Pan, J. Zou, X.D. Yao, Advanced Energy Materials 1 (2011) 387–393.
[3] L. Shao, C.H. Lau, S.L. Liu, D.R. Paul, J.Z. Xia, Y.C. Jean, H.M. Chen, T.S. Chung, Advanced Energy Materials 1 (2011) 634–642.
[4] F.J. DiSalvo, Science 285 (1999) 703–706.
[5] M.S. Dresselhaus, G. Chen, M.Y. Tang, R.G. Yang, H. Lee, D.Z. Wang, et al., Advanced Materials 19 (2007) 1043–1053.
[6] B.Z. Tian, X.L. Zheng, T.J. Kempa, Y. Fang, N.F. Yu, G.H. Yu, et al., Nature 449 (2007) 885–888.
[7] I. Gur, N.A. Fromer, M.L. Geier, A.P. Alivisatos, Science 310 (2005) 462–465.
[8] J.L. Mcnichols, W.S. Ginell, J.S. Cory, Science 203 (1979) 167–168.
[9] W.U. Huynh, J.J. Dittmer, A.P. Alivisatos, Science 295 (2002) 2425–2427.
[10] Q.B. Pei, G. Yu, C. Zhang, Y. Yang, A.J. Heeger, Science 269 (1995) 1086–1088.
[11] G. Yu, J. Gao, J.C. Hummelen, F. Wudl, A.J. Heeger, Science 270 (1995) 1789–1791.
[12] L. Shen, X. Zhang, E. Uchaker, C. Yuan, G. Cao, Advanced Energy Materials (2012), http://dx.doi.org/10.1002/aenm.201100720.
[13] L. Su, Y.X. Gan, Nano Energy 1 (2012) 159–163.
[14] S.M. Jafarian, P. Haseli, G. Karimi, International Journal of Energy Research 34 (2010) 946.
[15] G.J. Offer, J. Mermelstein, E. Brightman, N.P. Brandon, Journal of the American Ceramic Society 92 (2009) 763.
[16] L. Yang, S. Wang, K. Blinn, M. Liu, Z. Liu, Z. Cheng, M. Liu, Science 326 (2009) 126.
[17] Y.B. Kim, T.P. Holme, T.M. Gür, F.B. Prinz, Advanced Functional Materials 21 (2011) 4684–4690.
[18] W. Jiang, Y.C. Zhang, W. Woob, S.T. Tu, Journal of Power Sources 296 (2011) 10616–10624.
[19] M.C. Tucker, L. Cheng, Journal of Power Sources 196 (2011) 10074–10078.
[20] B. Timurkutluk, C. Timurkutluk, M.D. Mat, Y. Kaplan, Journal of Power Sources 196 (2011) 9361–9364.
[21] L.L. Zhang, T.M. He, Journal of Power Sources 196 (2011) 8352–8359.
[22] Y.S. Chou, J.W. Stevenson, Journal of Power Sources 191 (2009) 384–389.
[23] S.P. Jiang, Journal of Power Sources 183 (2008) 595–599.
[24] S. Huang, Q. Lu, S. Feng, et al., Advanced Energy Materials 1 (2011) 1094–1096.
[25] P.I. Cowin, C.T.G. Petit, R. Lan, et al., Advanced Energy Materials 1 (2011) 314–332.
[26] B. Liu, Bin, X. Chen, Y. Dong, et al., Advanced Energy Materials 1 (2011) 343–346.
[27] J.C. Ruiz-Morales, J. Canales-Vazquez, C. Savaniu, et al., Nature 439 (2006) 568–571.
[28] E.D. Wachsman, K.T. Lee, Science 334 (2011) 935–939.
[29] T. Suzuki, H. Zahir, F. Yoshihiro, et al., Science 325 (2009) 852–855.
[30] Y.H. Huang, R.I. Dass, Z.L. Xing, et al., Science 312 (2006) 254–257.
[31] K.J. Yoon, P. Zink, S. Gopalan, U.B. Pal, Journal of Power Sources 172 (2007) 39.
[32] K.R. Cooper, M. Smith, Journal of Power Sources 160 (2006) 1088.
[33] T. Hibino, A. Hashimoto, T. Inoue, J. Tokuno, S. Yoshida, M. Sano, Science 288 (2000) 2031.
[34] Y. Nie, W. Zhou, J. Sunarso, et al., Electrochemistry Communications 3 (2011) 1340–1343.
[35] Y.N. Kim, J.H. Kim, A. Manthiram, International Journal of Energy Research 36 (2011) 15295–15303.
[36] C. Su, W. Wang, H. Shi, et al., Journal of Power Sources 196 (2011) 7601–7608.
[37] A. Dutta, J. Mukhopadhyay, R.N. Basu, Journal of the European Ceramic Society 29 (2009) 2003–2011.

[38] M. Zunic, L. Chevallier, F. Deganello, et al., Journal of Power Sources 190 (2009) 417–422.
[39] D. Ding, L. Li, K. Feng, et al., Journal of Power Sources 187 (2009) 400–402.
[40] M. Muranaka, K. Sasaki, A. Suzuki, et al., Journal of the Electrochemical Society 156 (2009) B743–B747.
[41] G. Karimi, X. Li, P. Teertstra, Electrochimica Acta 55 (2010) 1619.
[42] M. Khandelwal, M.M. Mench, Journal of Power Sources 161 (2006) 1106.
[43] Z.P. Li, T. Mori, G.J. Auchterlonie, Y.N. Guo, J. Zou, J. Drennan, M. Miyayama, The Journal of Physical Chemistry C 115 (2011) 6877.
[44] A. Hauch, A. Georg, Electrochimica Acta 46 (2001) 3457.
[45] X. Yuan, H. Wang, J.C. Sun, J. Zhang, International Journal of Hydrogen Energy 32 (2007) 4365.
[46] K. Kerman, B.K. Lai, S. Ramanathan, Advanced Energy Materials 2 (2012) 1.
[47] K. Kerman, B.K. Lai, S. Ramanathan, Journal of Power Sources 202 (2012) 120.
[48] B.C.H. Steele, A. Heinzel, Nature 414 (2011) 345.
[49] D.W. Jung, K.L. Duncan, E.D. Wachsman, Acta Materialia 58 (2010) 355.
[50] F. Zhao, T.J. Armstrong, A.V. Virkar, Journal of the Electrochemical Society 150 (2003) A249–A256.
[51] W. He, K.J. Yoon, R.S. Eriksen, S. Gopalan, S.N. Basu, U.B. Pal, Journal of Power Sources 195 (2010) 532.
[52] W. He, B. Wang, H. Zhao, Y. Jiao, Journal of Power Sources 196 (2011) 9985.
[53] W. He, B. Wang, Advanced Energy Materials 2 (2012) 329.
[54] R.M. Ormerod, Chemical Society Reviews 32 (2003) 17–28.
[55] S. Tao, J.T.S. Irvine, Nature Materials 2 (2003) 320–323.
[56] A.B. Stambouli, E. Traversa, Renewable and Sustainable Energy Reviews 6 (2002) 433–455.
[57] O. Yamamoto, Electrochimica Acta 45 (2000) 2423–2435.
[58] F. Zhao, A.V. Virkar, Journal of Power Sources 141 (2005) 79–95.
[59] D.H. Jeon, Electrochimica Acta 54 (2009) 2727–2736.
[60] H. Matsumoto, I. Nomura, S. Okada, T. Ishihara, Solid State Ionics 179 (2008) 1486–1489.
[61] W. He, B. Wang, J.H. Dickerson, Nano Energy 1 (2012) 828–832.
[62] M. Liu, Y.M. Choi, L. Yang, K. Blinn, W. Qin, P. Liu, M. Liu, Nano Energy 1 (2012) 448–455.
[63] H.J. Choi, S.M. Jung, J.M. Seo, D.W. Chang, L. Dai, J.B. Baek, Nano Energy (2012). http://dx.doi.org/10.1016/j.nanoen.2012.05.001.
[64] M. Zhang, L. Dai, J.B. Baek, Nano Energy (2012), http://dx.doi.org/10.1016/j.nanoen.2012.02.008.
[65] J. Phattaranawik, R. Jiraratananon, A.G. Fane, Journal of Membrane Science 215 (2003) 75–85.
[66] R. Krishna, J.A. Wesselingh, Chemical Engineering Science 52 (1997) 861–911.
[67] A.S. Joshi, A.A. Peracchio, K.N. Grew, W.K.S. Chiu, Journal of Physics D: Applied Physics 40 (2007) 7593–7600.
[68] M. Cannarozzo, A.D. Borghi, P. Costamagna, Journal of Applied Electrochemistry 38 (2008) 1011–1018.
[69] J.W. Veldsink, G.F. Versteeg, W.P.M.V. Swaaij, R.M.J.V. Damme, The Chemical Engineering Journal and the Biochemical Engineering Journal 57 (1995) 115–125.
[70] B. Kenney, M. Valdmanis, C. Baker, J.G. Pharoah, K. Karan, Journal of Power Sources 189 (2009) 1051–1059.
[71] R. Suwanwarangkul, E. Croiset, M.W. Fowler, P.L. Douglas, E. Entchev, M.A. Douglas, Journal of Power Sources 122 (2003) 9–18.
[72] S.W. Webb, K. Pruess, Transport in Porous Media 51 (2003) 327–341.
[73] R. Jackson, Transport in Porous Catalysts, Elsevier, Amsterdam, 1977.
[74] C.L. Tsai, V.H. Schmidt, Journal of Power Sources 196 (2011) 692–699.
[75] W. Kong, H. Zhu, Z. Fei, Z. Lin, Journal of Power Sources 206 (2012) 171–178.
[76] W. Kast, C.R. Hohenthanner, International Journal of Heat and Mass Transfer 43 (5) (2000) 807–823.
[77] P. Kerkhof, Chemical Engineering Journal and the Biochemical Engineering Journal 64 (3) (1996) 319–343.
[78] L.M. Pant, S.K. Mitra, M. Secanell, Journal of Power Sources 206 (2012) 153–160.
[79] J.D. Ramshaw, Journal of Non-equilibrium Thermodynamics 15 (1990) 295–300.
[80] Z. Yu, R.N. Carter, Journal of Power Sources 195 (2010) 1079–1084.
[81] C. Chan, N. Zamel, X. Li, J. Shen, Electrochimica Acta 65 (2012) 13–21.
[82] J. Crank, The Mathematics of Diffusion, second ed., Oxford University Press, NY, 1975.
[83] T. Marrero, E. Mason, Journal of Physical and Chemical Reference Data 1 (1) (1972) 3–118.
[84] L.M. Pant, S.K. Mitra, M. Secanell, in: ASME 2011 9th International Conference on Nanochannels, Microchannels, and Minichannels, No. ICNMM2011-58181, Edmonton, Alberta, Canada, 2011.
[85] W. He, Advanced Energy Materials, aenm.201201113.
[86] J. Golbert, C.S. Adjiman, N.P. Brandon, Industrial & Engineering Chemistry Research 47 (2008) 7693–7699.
[87] S. Giraud, J. Canel, Journal of the European Ceramic Society 28 (2008) 77–83.
[88] B. Iwanschitza, L. Holzerb, A. Maia, M. Schütze, Solid State Ionics 211 (2012) 69–73.
[89] W. He, B. Wang, Journal of Power Sources 232 (2013) 93–98.